Reac Kinet Mech Cat (2015) 115:499–512
DOI 10.1007/s11144-015-0853-0

Effect of drying conditions on the textural, structural and catalytic properties of Cr/ZrO_2–SO_4: *n*-hexane conversion

Sahar Raissi[1] · Nesrine Kamoun[1] · Mohamed Kadri Younes[1] · Abdelhamid Ghorbel[1]

Received: 10 November 2014 / Accepted: 10 March 2015 / Published online: 19 March 2015

Abstract Aerogel and xerogel catalysts based on sulfated zirconia doped with chromium are prepared by sol–gel method. The effects of drying mode and calcination temperature are reflected in the characteristics of the final solids. The addition of chromium to aerogel sulfated zirconia not only provides an important development of the specific surface area from 100 to 213 $m^2\ g^{-1}$; but also stabilizes a pure metastable ZrO_2 tetragonal phase in a large calcination temperature domain. In addition, the aerogels develop active sulfate groups and preserve them on the surface even at high heating. Those characteristics contribute to the improvement of catalytic performances of sulfated zirconia in *n*-hexane conversion. However, in the case of xerogels, the increase of temperature treatment leads to the loss of sulfate active groups and porosity destruction which make them completely inactive in spite of the development of ZrO_2 tetragonal phase.

Keywords Sulfated zirconia · Chromium · Conversion of *n*-hexane

Introduction

Heavy naphtha constitutes a considerable portion of petroleum products. However, it is essential to treat this portion in order to improve its characteristics and transform it into valuable products such as plastic chemicals and liquid petroleum gases (LPG) issued principally by cracking light naphtha into propylene and ethylene and liquefied high octane gasoline obtained by the isomerization of light alkanes [1]. The skeletal isomerization of light alkanes is known to be catalyzed by

✉ Sahar Raissi
r.sahar@hotmail.fr

[1] Laboratoire de Chimie des Matériaux et Catalyse, Faculté des Sciences de Tunis, Université de Tunis El Manar, 2092 Tunis, Tunisia

acid catalysts [2]. Acid solids like zeolite and sulfated oxides are attracting the interest of researchers and even industries [3–5]. Platinum or other metals associated to sulfated zirconia have already been studied in our laboratory. The results revealed that this catalytic system is very performing [6–9]. Thanks to their hydrogenating–dehydrogenating and redox properties, transition metals can constitute an interesting alternative to the expensive platinum [10–12]. Good control of the preparation conditions is decisive. The sol–gel method is one of the methods well-known for the homogeneity that it offers to solids. When it is associated to super critical drying, the sol–gel procedure favors the development of surface area thanks to development of a nanocrystalline particles [12, 13].

In this work, chromium was chosen as a doping metal of sulfated zirconia because of its redox and hydrogenating–dehydrogenating properties. In fact, it improves stability of this catalyst in *n*-alkane conversion reactions. We, particularly, focus our attention on the evaluation of the repercussions of some preparation conditions such as calcinations temperature and drying mode on catalytic properties of those solids. The choice of this metal and the adoption of sol–gel method coupled to a supercritical drying provide promising catalysts, which are characterized by a developed texture, a stable crystalline structure and enhanced catalytic performances.

Experiments

Catalysts preparation

The solids were prepared following a sol–gel procedure. Zirconium propoxide (ALDRICH, 70 % in propanol) was dissolved in 1-propanol (ACROS 99 %). Sulfate groups were introduced from concentrated sulfuric acid (ACROS 96 %) with a molar ratio $n\mathrm{S}/n\mathrm{Zr} = 0.5$. Chromium acetylacetonate (ACROS 97 %) was added with a proportion $n\mathrm{Cr}/n\mathrm{Zr}$ equal to 0.1. The gel was obtained by addition of pure water to the alcoholic solution in the hydrolysis ratio $n(\mathrm{H_2O})/n\mathrm{Zr} = 3$. Then the mixture was kept at room temperature until the gelification. Once the gel formed, it was divided into two parts: one was dried in an autoclave under supercritical conditions of the solvent (536.6 K, 51 bar) to provide the aerogel and the other was dried under atmospheric pressure at 383 K to obtain the xerogels. The obtained solids were calcined under a flow of oxygen at 673 and 973 K with a heating rate of 3 K min^{-1} during 3 h. Aerogels are designed as AZSCrT and xerogels as XZSCrT with T = 673 K or T = 973 K.

Sample characterization

Textural characterization was performed by a Micromeritics apparatus ASAP 2000, monitored by a computer. Samples were first degassed for 4 h under vacuum at 473 K. Fifty point adsorption and desorption isotherms of $\mathrm{N_2}$ were obtained, from which the specific surface area and pore size distribution were determined respectively by BET and BJH methods [14, 15].

XRD patterns were recorded on an automatic Philips Panalytical diffractometer using Cu K_α radiation ($\lambda = 1.54056$ Å) and nickel monochromator. The reticular distances calculated are compared to those given by the Joint Committee on Powder Diffraction Standards (JCPDS 17-0923). The crystallite size of zirconia tetragonal phase was determined from the characteristic peak [$2\theta = 30.188$ for the (1 1 1) reflection] using the Scherrer equation $L = K\lambda/b \cos\theta$, where $K = 1$, L represents the crystallite size, λ the wavelength of Cu $K_{\alpha 1}$ radiation and b the corrected half width of the diffraction peak [16].

IR spectra were recorded at resolution 2 cm^{-1} with a Perkin Elmer FTIR spectrophotometer over a range of 4000–300 cm^{-1} in the transmission mode. The samples were prepared by dilution in KBr and pressed to form discs.

UV–Visible spectra were recorded on a Perkin Elmer spectrophotometer lambda 45 coupled to an integration sphere RSA-PE-20 in the range 200–900 nm with a speed of 960 nm min^{-1} and an aperture of 4 nm.

XPS spectra were obtained using a VG Escalab 220XL spectrometer. The source is monochromatic Al K_α radiation (1486.6 eV, 100 W). The size of diameter spot is 500 μm and electromagnetic lens mode works with pass energy of 30 eV.

The C1s (285.0 eV) binding energy (BE) was used as internal reference and photopeaks identification was carried out using Casa XPS software.

Catalytic reaction

The isomerization of *n*-hexane was carried out in a U-shaped tubular reactor operating at atmospheric pressure between 423 and 493 K. A sample of 100 mg catalyst was put in contact with *n*-hexane (20 Torr) diluted in H_2 at a flow rate of 30 mL min^{-1}. The reactant and reaction products are detected and analyzed with an on-line chromatography unit with a squalane on spherosil column and a FID detector.

Results and discussion

Crystalline phase

The XRD results, summarized in Table 1, show that only the aerogel is crystallized and develop the ZrO_2 tetragonal phase for a calcination temperature of 473 K. In fact, the aerogel procedure, as reported by Blido et al. [13], is suitable for the formation of nanosolids which contribute to the stabilization of the unstable tetragonal polymorphism at low temperature. This result is confirmed by the examination of the DRX patterns. At a calcination temperature of 973 K, aerogel and xerogel develop the ZrO_2 tetragonal phase however, the crystallite size of XZSCr973 (9.56 nm) is slightly greater than the AZSCr973 one (8.70 nm). Furthermore, it is important to emphasize the key role played by chromium for the stabilization of this phase in agreement with previous study on chromium supported

Table 1 DRX and N_2 physisorption results of the aerogel and xerogel catalysts calcined at 673 and 973 K

Calcination temperature (K)	Aerogels						Xerogels			
	$Size_{Cri}$ (nm)	Crystal phase	S_{BET} ($m^2\ g^{-1}$)	D_p (Å)	V_p ($cm^3\ g^{-1}$)	$Size_{Cri}$ (nm)	Crystal phase	S_{BET} ($m^2\ g^{-1}$)	D_p (Å)	V_p ($cm^3\ g^{-1}$)
673	3.96	Tetragonal	213	176	0.94	–	Amorphous	39	35–78	0.05
973	8.70	Tetragonal	133	195	0.64	9.26	Tetragonal	131	35–95	0.15

by zirconia [17]. Chromium, in opposition to other metals such as nickel [12], can be anchored into the sulfated zirconia lattice which preserves the crystallite growth and consequently stabilizes a pure ZrO_2 tetragonal phase for a large domain of temperatures.

Textural characterization

Textural characterization was evaluated from nitrogen adsorption–desorption isotherms at 77 K. Both aerogels and xerogels exhibit the type IV isotherm with H3 loop, which is characteristic of mesoporous solids with tubular and cylindrical pores [18]. However, the comparison of the surface area and the porosity of the two types of solids reveal that they present clear differences. Table 1 reveals that when solids are calcined at the same temperature, aerogels are characterized by specific surface areas higher than xerogels, which are directly related to the drying mode. In fact, the evacuation of the solvent under atmospheric conditions creates on the surface of the gel a liquid–vapor interface which causes the formation of a concavity on the pores of the gels. The increase of the compression forces caused by this concavity on the walls causes their shrinkage and even their destruction [19].

The exploitation of the calcination temperature effect on the two types of solids showed that the behavior of solids differs according to the drying mode (Table 1). While the xerogel specific surface area increases considerably with the calcination temperatures, the aerogel shows an important fall. The increase of xerogel surface can be explained by the development of the ZrO_2 tetragonal phase. However, the pore volumes of these solids remain practically unchanged and negligible compared to the aerogels ones. On the contrary, the decrease of the aerogels S_{BET} is mainly related to a sintering phenomenon and also to a loss of a part of sulfate groups. This result is accompanied by a decrease of the pores volume and an enlargement of the pores. A similar result was reported by Vaudagna [20] that put the accent on the role of sulfate in the preservation of the specific surface area.

The pore size distribution of solids is also affected by the drying mode. For aerogels, the pore type is homogenous and centered at 176 Å for AZSCr673 and at 196 Å for AZSCr973. However, the crystallite size determined by the Scherrer formula for those solids is 3.96 and 8.70 nm. Thus, this porosity is inter-granular. For xerogels even the pore volume is very modest, they present some pores of two types. The first type has a diameter of 35 Å and the second is in the range 78–90 Å. A similar result was found by Amairia et al. [21]. The existence of two types of pores can result from a partial destruction of pores.

FTIR spectroscopy

IR spectra are presented in Fig. 1. This characterization technique reveals some differences between the solids investigated concerning the nature and the retention of sulfate groups. The region of hydroxyl groups seems also affected by the drying mode as well as by the calcination temperature.

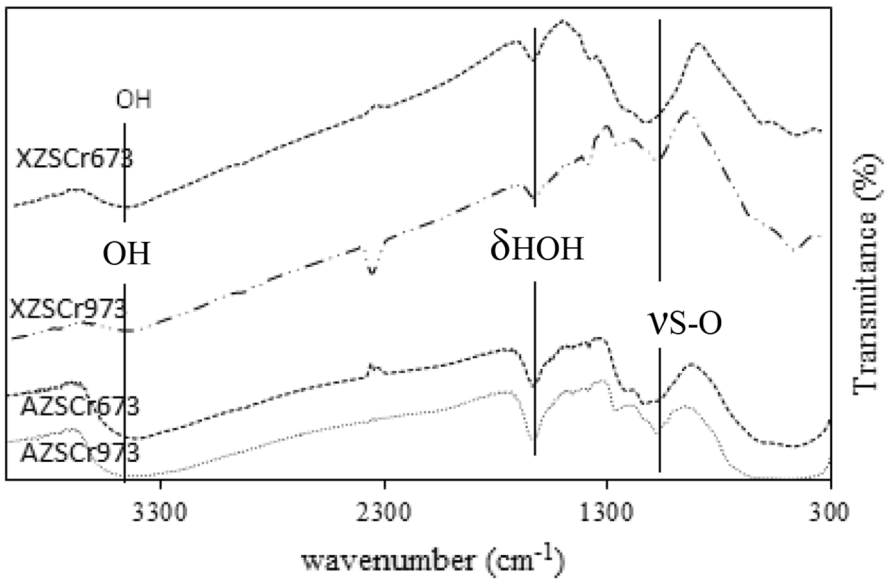

Fig. 1 IR spectra of sulfated zirconia doped with chromium aerogels calcined at 673 K (AZSCr673) at 973 K (AZSCr973) and xerogels calcined at 673 K (AZSCr673) at 973 K (AZSCr973)

The spectra of the different solids are characterized by a peak at 1620 cm^{-1}, characteristic of non-dissociated water molecules (δ_{HOH}) [22]. This peak is very intense in the aerogel case indicating that water is more adsorbed on the surface of solids thanks to their developed porosity as shown by textural characterization.

The wide band, relative to the vibration of hydroxyl group on chromate groups at 3400 cm^{-1} [22–24], is well noticeable in the case of aerogels. However, in the case of xerogels, it becomes less intense and is shifted to 3440 cm^{-1}. This could be probably due to differences in the nature of Brønsted acidic sites related to the water adsorption in pores with different size in the two kinds of solids. On the other hand, the retention and the nature of sulfates seem to be affected by the drying mode. The region situated between 1000 and 1300 cm^{-1} is relative to the sulfate groups, all the spectra present a large peak centered at 1062 cm^{-1} with a shoulder at 1112 cm^{-1} that becomes well resolved for the catalysts calcined at 973 K, which are assigned to ν_{S-O} in $S_2O_7^{2-}$ and $S_2O_7^{2-}nH_2O$, respectively [24, 25]. Those bands are more intense in the aerogel and at high calcination temperature. Those bands reveal the appearance of covalent species on the crystallographic defaults on the tetragonal zirconia which confer to the solids an enhancement of the catalytic properties [26].

UV–Visible spectroscopy

The UV–Visible spectra of all the catalysts are summarized in Fig. 2. They show several bands situated at 260, 287, 350 and 380 nm, which can be attributed to the charge transfer of $O^{2-} \rightarrow Cr^{6+}$ [27]. Moreover, these bands are characterized by an important multiplicity, which reveals the presence of many types of Cr^{6+} ions

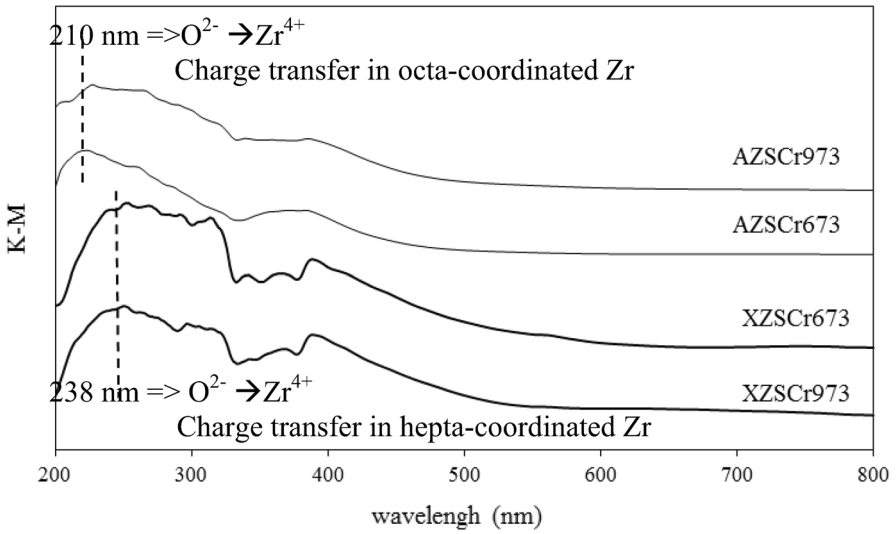

Fig. 2 UV–Visible spectra of sulfated zirconia doped with chromium aerogels calcined at 673 K (AZSCr673) at 973 K (AZSCr973) and xerogels calcined at 673 K (AZSCr673) at 973 K (AZSCr973)

existing in different symmetry or with different length of the Cr–O bond as monochromate and bichromate species [27]. It seems like neither the calcination temperature nor the drying mode affects the oxidation state of chromium VI. This result was observed by other authors for chromium supported by several types of solids [27–29].

However, the drying mode effect is mainly observed on the coordination number of zirconium. It is reported by Castellon [30] that the band, relative to the charge transfers $O^{2-} \rightarrow Zr^{4+}$, is shifted to the high energies when the Zr^{4+} coordination number increases. Thus the aerogel spectra are characterized by a band situated at around 210 nm which indicate that Zr^{4+} is octa-coordinated, however, the xerogels ones are characterized by a band at 238 nm, suggesting that Zr^{4+} is hepta-coordinated.

XPS spectroscopy

While UV–Visible spectroscopy shows chromium as only Cr(IV), XPS spectroscopy reveals the presence of some amount of Cr(III) on the surface of the catalysts. In fact, the Cr2p photopeak can be decomposed into two components centered at 576.0 and 578.4 eV related to Cr^{3+} and Cr^{6+}, respectively [31]. The ratio Cr^{3+}/Cr^{6+} increase in the aerogels from 1.1 to 1.5 with the calcination temperature (Fig. 3). The Zr3d5/2 photopeak is centered at a BE of 182.9 eV for all the solids (Fig. 4). This can be assigned to Zr^{4+} oxidation state in ZrO_2 oxide form [32]. The bad resolution of this peak in the case of AZSCr673 can be related to the poor crystallinity of this solid. The O1s photopeak is centered at 530.5 eV in XZSCr973 and it reveals that oxygen of the surface of this solid is mainly from ZrO_2 (Fig. 5). However, in the case of aerogels, this peak is asymmetrical and could

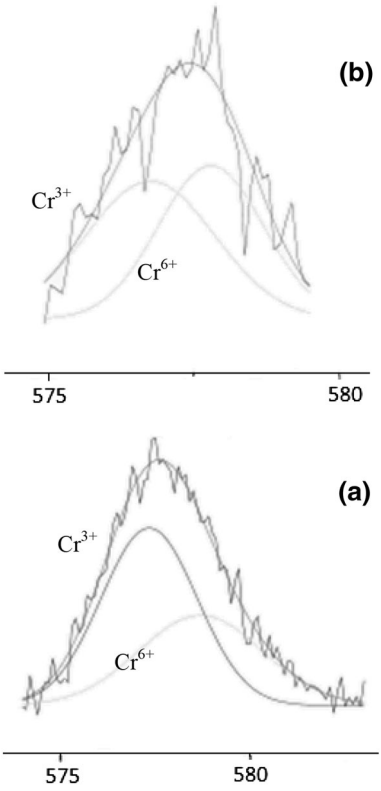

Fig. 3 XPS spectra of Cr2p region revealing the presence of Cr^{3+} and Cr^{6+} in aerogels sulfated zirconia doped with chromium calcined at **a** 673 K and **b** 973 K

be decomposed into two species, the major one with BE of 530.5 eV and the second one with BE of 532.2 eV [25] due to oxygen of the sulfate species, which increases with the calcination temperature.

n-Hexane isomerization reaction

The study of the *n*-hexane isomerization reaction between 423 and 493 K reveals that xerogels are completely inactive in this range. However, aerogels exhibit a good activity that increases with calcination temperature (Fig. 6). These catalytic properties can be related to the particular physico-chemical characteristics conferred to the aerogels due to drying under supercritical conditions. However, the inappropriate texture can be responsible of the inactivity of xerogels. The presence of pores of small diameter (35 Å) can provoke an accumulation of cokes and blocks the access to active sites. Thus, even the development of the active ZrO_2 tetragonal phase on the xerogel calcined at 973 K, it is still completely inactive [33].

The analysis of the catalytic test results of *n*-hexane conversion (Table 2) revealed that no dibranched isomers were obtained and no alkane longer than six

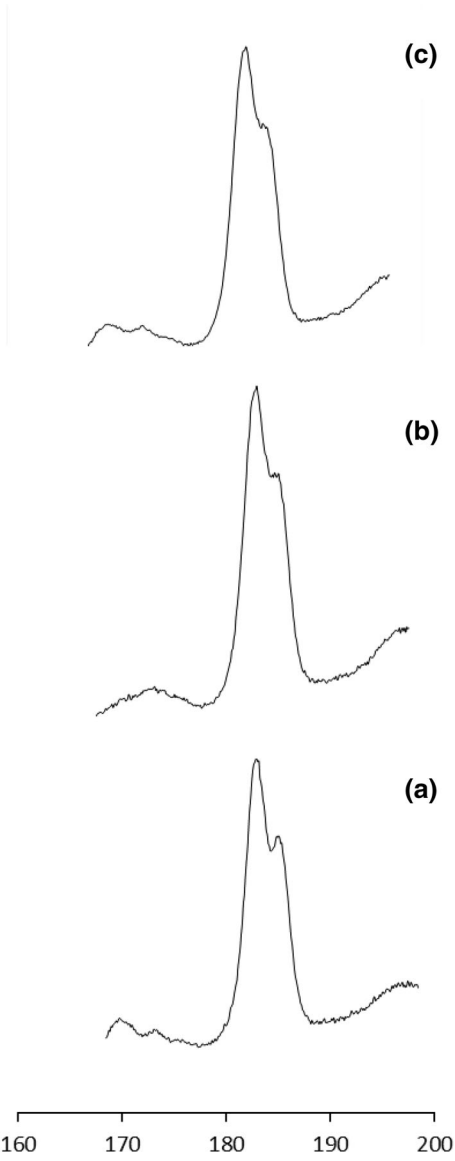

Fig. 4 XPS spectra of Zr2p region revealing a better crystallinity in the case of sulfated zirconia doped with chromium xerogel calcined at **a** 973 K than in aerogels ones calcined at **b** 973 K, **c** 673 K because of resolution of this peak

carbons was detected. These findings suggest that the isomerization involves via a monomolecular mechanism [34], which consists of the rearrangement of a protonated cyclopropane intermediate. Chromium, especially when it is in "oxo sites", facilitates the appearance of hexene that engenders easily a carbenium which gives cyclopropane intermediate on the acid sites of the sulfated zirconia (Fig. 7). Similar observations were reported by Kamoun et al. [35] in the case of sulfated zirconia doped with nickel and by Wan et al. [36] when it is doped with iron.

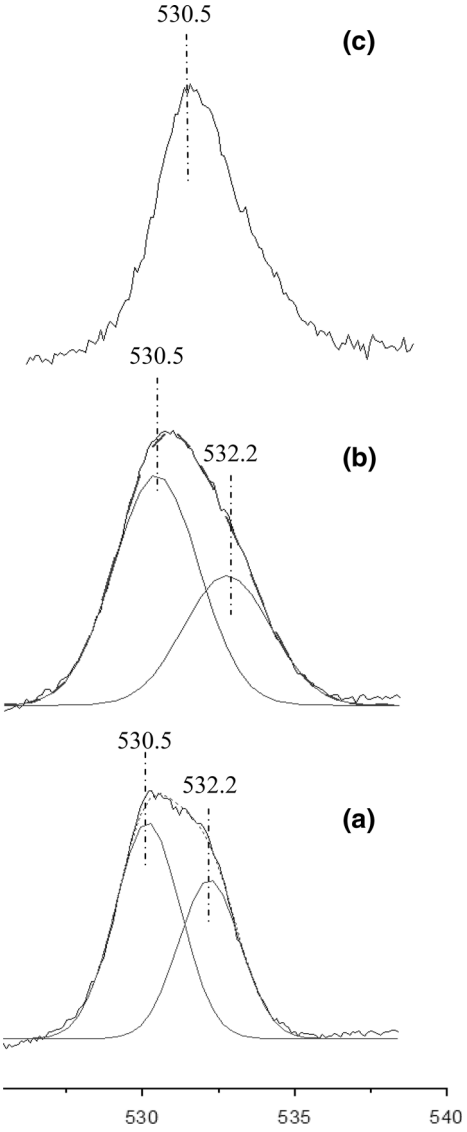

Fig. 5 XPS spectra of O1s region revealing the presence of two types of oxygen belonging to Metal-O (530.0 eV) and Soufre-O (532.2 eV) in sulfated zirconia doped with chromium aerogels calcined at **a** 973 K, **b** 673 K and xerogel calcined at **c** 973 K

The XPS study shows greater presence of chromium "oxo sites" on the surface of the aerogel calcined at high temperature, which explains its catalytic performances improvement mainly at the level of stability. Even the presence of those species, xerogel XZSCr973 remains inactive. It seems that the activity require the chromium in "oxo sites" and the sulfate groups.

Indeed, we are persuaded that the species responsible of the activity are almost the sulfates characterized by O1s photopeak centered at 532.2 eV. Similar

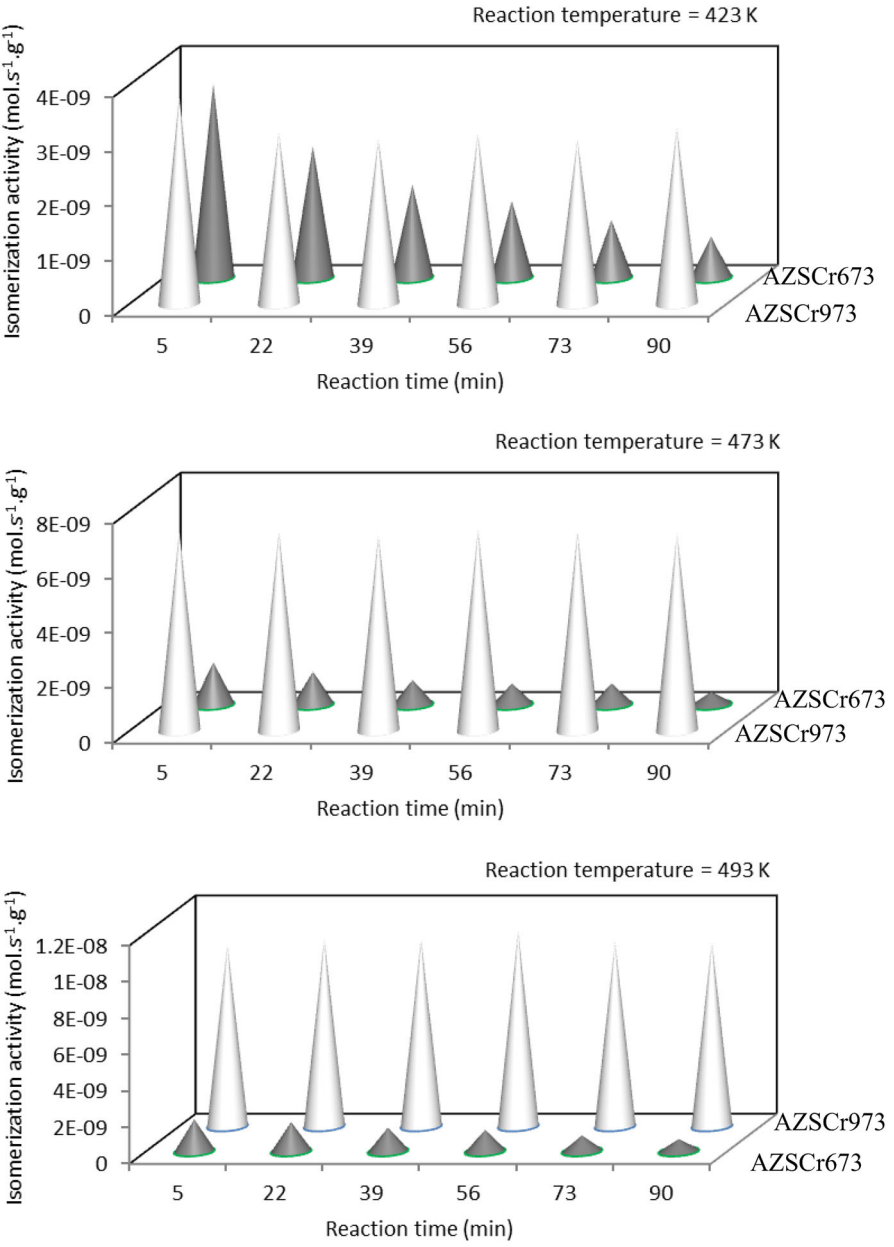

Fig. 6 Activity of *n*-hexane hydro-isomerization in mol g^{-1} s^{-1} versus reaction time at different temperatures of 100 mg of sulfated zirconia aerogels calcined at **a** 973 K and **b** 673 K

findings were reported by Kamoun et al. [35] in the case of sulfated zirconia doped with nickel and in a previous work in the case of sulfated zirconia doped with cobalt [37].

Table 2 Selectivity of products of *n*-hexane conversion (%)

	Isomerisation selectivity (%)		Cracking selectivity (%)		
	M2P	M3P	Ethane	Propane	Isobutane
AZSCr673					
423	20.5	16.0	30.5	0	33.0
443	19.1	13.0	33.2	0	34.7
473	16.0	15.1	35.8	0	33.1
493	8.4	7.2	40.0	0	44.4
AZSCr973					
423	40.2	33.3	11.0	6.5	9.0
443	35.4	29.4	16.0	7.2	12.0
473	33.2	30.4	14.3	10.4	11.7
493	32.1	28.0	17.1	9.9	12.9

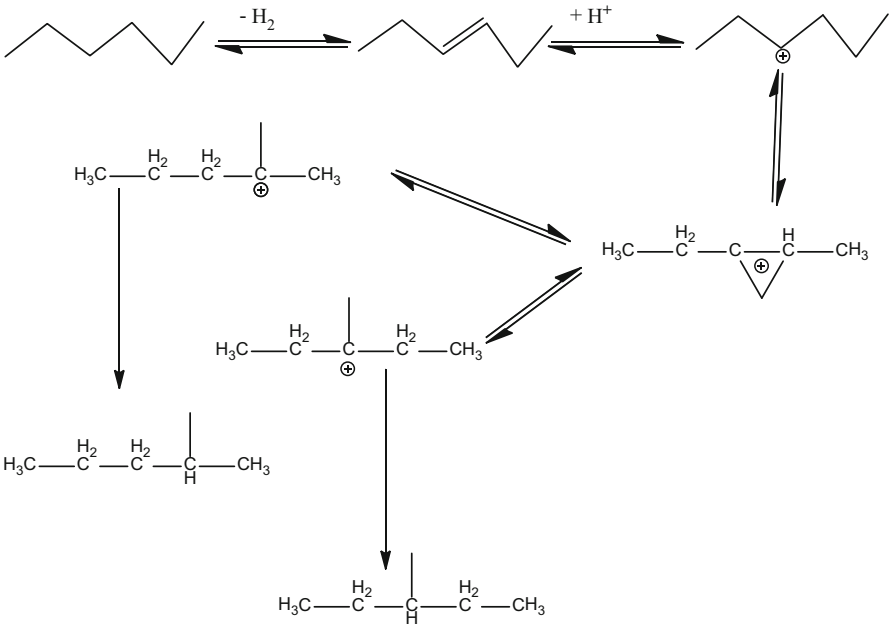

Fig. 7 Isomerization mechanism of *n*-hexane on bifunctionnal sulphated zirconia doped with chromium

Conclusion

Promotion of sulfated zirconia with chromium and drying under supercritical solvent conditions improve the properties of this catalyst. The S_{BET} increases from 100 to 200 $m^2\ g^{-1}$ and the metastable ZrO_2 tetragonal phase is preserved for a large

domain of calcination temperature from 673 to 973 K. Moreover, spectroscopic study reveals the presence of active sulfate groups and chromium "oxo species" which are stabilized at high calcination temperature. Those properties enhance considerably the catalytic performances in the *n*-hexane conversion. However, the drying solvent under atmospheric conditions seems to be unfavorable to the development of the active species because it provokes apparition of small diameter pores. The latter are easily blocked by coke deposition and do not ensure a direct access to active sites.

References

1. Yamaguchi A, Jin D, Ikeda T, Sato K, Hiyoshi N, Hanaoka T, Mizukami F, Shirai M (2014) Deactivation of ZSM-5 zeolite during catalytic steam cracking of *n*-hexane. Fuel Process Technol 126:343–349
2. Bardin BB, Davis RJ (1998) A comparison of cesium-containing heteropolyacid and sulphated zirconia catalysts for isomerization of light alkanes. Top Catal 6:77–86
3. Hino M, Kobayashi S, Arata K (1979) Solid catalyst treated with anion. 2. Reactions of butane and isobutane catalyzed by zirconium oxide treated with sulfate ion. Solid superacid catalyst. J Am Chem Soc 101:6439–6441
4. Davis BH, Keogh RA, Srinivasan R (1994) Sulfated zirconia as a hydrocarbon conversion catalyst. Catal Today 20:219–256
5. Watanabe K, Chiyoda N, Kawakami T (2008) The Saudi Arabia–Japan Joint Symposium, Dhahran, 16–17 Nov
6. Younes MK, Ghorbel A, Rives A, Hubaut R (2000) Characterization and catalytic properties of aerogels sulfated zirconia. Stud Surf Sci Catal 130:3219–3224
7. Akkari R, Ghorbel A, Essayem N, Figueras F (2007) Synthesis and characterization of mesoporous silica-supported nano-crystalline sulfated zirconia catalysts prepared by a sol–gel process: effect of the S/Zr molar ratio. Appl Catal A 328:43–51
8. Ben Hamouda L, Ghorbel A, Figueras F (2000) Study of acidic and catalytic properties of sulfated zirconia prepared by sol–gel process: influence of preparation conditions. Stud Surf Sci Catal 130:971–976
9. Méjri I, Younes MK, Ghorbel A (2006) Comparative study of the textural and structural properties of the aerogel and xerogel sulphated zirconia. J Sol–Gel Sci Technol 40:3–8
10. Blekkan EA, Johnsen KA, Loften T (2005) Isomerization of light alkanes: preparation and characterization of platinum promoted sulfated zirconia catalysts. React Kinet Catal Lett 86:149–155
11. Raissi S, Younes MK, Ghorbel A, Garin F (2010) Effect of sulphate groups on catalytic properties of chromium supported by zirconia in the *n*-hexane aromatization. J Sol–Gel Sci Technol 53(2): 412–417
12. Kammoun N, Younes MK, Ghorbel A, Mamede A, Rives A (2014) Comparative study of the texture and structure of aerogel and xerogel sulphated zirconia doped with nickel. J Porous Mater 19: 375–382
13. Bedilo AF, Klabunde KJ (1997) Synthesis of high surface area zirconia aerogels using high temperature supercritical drying. Nanostruct Mater 8:119–135
14. Brunauer S, Emmett PH, Teller E (1938) Adsorption of gases in multimolecular layers. J Am Chem Soc 60:309–319
15. Barrett ED, Joyner LG, Halenda PP (1951) The determination of pore volume and area distributions in porous substances. J Am Chem Soc 73:373–380
16. Rietveld HM (1969) A profile refinement method for nuclear and magnetic structures. J Appl Crystallogr 2:65–71
17. Raissi S, Younes MK, Ghorbel A (2009) Etude comparative des propriétés texturales et structurales de la zircone dopée au chrome a l'état aérogel et xérogel. Ann Chim 34(1):11–20

18. Rouquerol J, Avnir D, Fairbridge CW, Everett DH, Haynes JH, Pernicone N, Ramsay JDF, Sing KSW, Unger KK (1994) Recommendations for the characterization of porous solids. Pure Appl Chem 66:1739–1758
19. Schneider M, Baiker A (1995) Aerogels in catalysis. Catal Rev 37:515–556
20. Vaudagna SR, Comelli RA, Fıgoli NS (1996) Influence of the preparation conditions on the textural properties and *n*-hexane isomerization activity of $Pt/SO_4^{2-}–ZrO_2$. React Kinet Catal Lett 58:111–112
21. Amairia C, Fessi S, Ghorbel A, Rives A (2010) Methane oxidation behaviour over sol–gel derived $Pd/Al_2O_3–ZrO_2$ materials: influence of the zirconium precursor. J Mol Catal A 332:25–31
22. Babou F, Coudurier G, Vedrine JC (1995) Acidic properties of sulfated zirconia: an infrared spectroscopic study. J Catal 152:341–349
23. Ahmed MA (2011) Surface characterization and catalytic activity of sulfated-hafnia promoted zirconia catalysts for *n*-butane isomerization. Fuel Process Technol 92:1121–1128
24. Klose BS, Jentoft FC, Schlögl R (2005) In situ diffuse-reflectance infrared spectroscopic investigation of promoted sulfated zirconia catalysts during *n*-butane isomerization. J Catal 233:68–80
25. Kamoun N, Younes MK, Ghorbel A, Mamede AS, Rives A (2014) Effect the solvent evacuation mode on the catalytic properties of nickel-modified sulfated zirconia catalysts: *n*-hexane isomerization. Reac Kinet Mech Cat 111:199–214
26. Morterra C, Cerrato G, Pinna F, Signoretto M (1995) Crystal phase, spectral features, and catalytic activity of sulfate-doped zirconia systems. J Catal 157:109–123
27. Fujdala Kyle L, Tilley TD (2003) Thermolytic molecular precursor routes to Cr/Si/Al/O and Cr/Si/Zr/O catalysts for the oxidative dehydrogenation and dehydrogenation of propane. J Catal 218: 123–134
28. Korhonen ST, Airaksinen SMK, Bañares MA, Krause AOI (2007) Isobutane dehydrogenation on zirconia-, alumina-, and zirconia/alumina-supported chromia catalysts. Appl Catal A 333:30–41
29. Weckhuysen BM, Wachs IE, Schoonheydt RA (1996) Surface chemistry and spectroscopy of chromium in inorganic oxides. Chem Rev 96:3327–3350
30. Castellon ER, Lopez AJ, Torres PM (2003) Textural and structural properties and surface acidity characterization of mesoporous silica–zirconia molecular sieves. J Solid State Chem 175:159–169
31. Deng S, Li H, Li S, Zhang Y (2007) Activity and characterization of modified Cr_2O_3/ZrO_2 nanocomposite catalysts for oxidative dehydrogenation of ethane to ethylene with CO_2. J Mol Catal A 268:169–175
32. Resofski G, Muhler M, Sprenger S, Wild U, Paál Z (2003) Electron spectroscopy of sulfated zirconia, its activity in *n*-hexane conversion and possible reasons of its deactivation. Appl Catal A 240:71–77
33. Zarubica AR, Miljkovic MN, Kiss EE, Boskovic GC (2007) Benefits of mesopores in sulfated zirconia catalyst. React Kinet Catal Lett 90:145–150
34. Cheung TK, Gates BC (1998) Sulfated zirconia and iron- and manganese-promoted sulfated zirconia: do they protonate alkanes? Top Catal 6:41–47
35. Kamoun N, Younes MK, Ghorbel A, Mamede AS, Rives A (2015) Comparative study of aerogels nanostructured catalysts: $Ni/ZrO_2–SO_4^{2-}$ and $Ni/ZrO_2–Al_2O_3–SO_4^{2-}$. Ionics 21:221–229
36. Wan KT, Khouw CB, Davis ME (1996) Studies on the catalytic activity of zirconia promoted with sulfate, iron, and manganese. J Catal 158:311–326
37. Raissi S, Younes MK, Ghorbel A (2014) Mesoporous aerogels and xerogels based on sulphated zirconia doped with cobalt as hexane isomerization catalysts. J Mater Sci Eng 4(3):105–111